Supersonic Ionization Wave Driven by Radiation Transport in a Short-Pulse Laser-Produced Plasma

T. Ditmire, E. T. Gumbrell, R. A. Smith, L. Mountford, and M. H. R. Hutchinson
Blackett Laboratory, Imperial College of Science Technology and Medicine, London SW7 2BZ, United Kingdom
(Received 5 February 1996)

Through the use of an ultrashort (2 ps) optical probe, we have time resolved the propagation of an ionization wave into solid fused silica. This ionization wave results when a plasma is created by the intense irradiation of a solid target with a 2 ps laser pulse. We find that the velocity of the ionization wave is consistent with radiation driven thermal transport, exceeding the velocity expected from simple electron thermal conduction by nearly an order of magnitude. [S0031-9007(96)00542-X]

PACS numbers: 52.50.Jm, 52.25.Fi, 52.40.Nk, 52.70.Kz

Progress in understanding the interaction of intense, ultrashort laser pulses with plasmas has been quite dramatic in the previous decade [1]. This progress has been fueled by a desire to study plasma conditions at very high temperatures and electron densities, a condition made possible by the development of intense picosecond lasers which can rapidly heat a plasma before significant hydrodynamic expansion can take place [2]. Understanding of the physics behind energy transport mechanisms in these plasmas is central to these studies. This is not only because of the fundamental nature of these mechanisms to the understanding of plasma physics in general, but also because a clear picture of energy transport is required to fully understand the dynamics of ultrashort pulse x-ray generation [3], a very important application of short-pulse produced plasmas [4].

One important ultrafast process driven by energy transport is the formation of an ionization wave that propagates with a supersonic velocity into the solid after the target surface has been heated by an intense short pulse [5]. This process has been studied previously at intensities of $<5 \times 10^{14}$ W/cm^2 where the plasmas formed exhibited temperatures of 50 eV or less [6]. In these studies the velocity of the ionization wave was inferred from the Doppler shift exhibited by a probe beam reflected off the expanding ionization front within the cold fused silica substrate. This experiment found that the velocity of the ionization wave could be well explained by standard electron thermal conduction in this low intensity regime.

In this Letter we report the first time resolved measurements of the spatial extent of an ionization wave produced with high intensity (up to 10^{17} W/cm^2) picosecond pulses. At this intensity we find that the velocity of the ionization wave cannot be explained by simple electron thermal conduction. We find that our measurements are, instead, consistent with radiative thermal conduction. The resulting velocity and depth of penetration of the radiatively driven ionization wave is 1 to 2 orders of magnitude greater than that observed at low intensity. Previous measurements of radiative transport effects have been largely composed of long pulse ($\sim$1 ns) studies where the effects of radiative transport have been inferred by indirect means [7] or by direct measurement of radiative transport effects in thin foils [8,9] or foams [10] driven by a separate laser-created x-ray source. In these experiments the drive laser pulse width was comparable to or longer than the time scale for the energy transport. Our experiment represents the first direct measurement of radiative transport effects in short-pulse produced plasmas.

The energy flow in a high temperature plasma can take place by either electron or radiative transport. Radiative transport will dominate over electron thermal transport at high temperatures when a significant amount of the energy contained in the plasma is emitted as radiation in the UV and x-ray regions. We can estimate the parameters required for radiative transport to dominate over electron collisional transport by comparing the relative heat conductivity of the two mechanisms. We can estimate the electron thermal conductivity by using the Spitzer-Härm conductivity, $\kappa_{\mathrm{SH}} = 4k_B(k_BT_e)^{5/2}/m_e^{1/2}(Z+1)e^4 \ln\Lambda$ [11] (where m_e is the electron mass, e is the electron charge, k_BT_e is the electron thermal energy, and $\ln\Lambda$ is the Coulomb logarithm). The radiative thermal conductivity is, in general, a complicated function of the material opacity. It can be simply estimated, however, by using $\kappa_{\mathrm{rad}} = 16\sigma T_e^3\lambda_R/3$ [12] (where σ is the Stefan-Boltzman constant). Here λ_R is the Rossland, radiation mean free path. For an ionized plasma, this mean free path is roughly $\lambda_R \approx 9 \times 10^6 T_e^2/Z^2 n_i$ (for hydrogenic ions) [12]. Thus the ratio of the radiative thermal conductivity to the electron thermal conductivity is

$$\frac{\kappa_{\mathrm{rad}}}{\kappa_{\mathrm{SH}}} \approx 5 \times 10^{18} \frac{(k_BT_e)^{5/2}}{n_e}, \qquad (1)$$

where k_BT_e is given in eV (and we have taken $n_e = Zn_i$). Equation (1) implies that for a solid density plasma with an electron density of approximately 10^{23} cm^{-3} radiative heat transport will dominate when $k_BT_e >$ 100 eV. Therefore, we expect that radiative transport will dominate in the solid density, high temperature (500–1000 eV) plasmas created by an intense short pulse, as in our experiments.

 0031-9007/96/77(3)/498(4)$10.00

The experimental setup to measure the dynamics of the ionization wave inside a solid target is illustrated in Fig. 1. The experiment uses pulses from a Nd:glass laser based on chirped pulse amplification operating at 1054 nm. The laser produces pulses with a temporal width of approximately 2 ps and a pulse energy of up to 0.5 J. These pulses are focused with an $f/10$ lens, producing a focal spot of 20 μm and a peak intensity of up to 1×10^{17} W/cm^2. The circularly polarized pulses are focused at normal incidence onto the polished edge of a fused silica glass plate with a width of approximately 500 μm. Transparent fused silica is used as a target since it allows optical probing of the material beneath the surface of the target.

A small amount of energy is extracted from the main beam after compression with a 5% beam splitter to generate the probe pulse. The 1054 nm light is frequency doubled in KDP and then Raman shifted in ethanol to 620 nm. This wavelength shifting is required since probing with 1054 nm light or frequency doubled light at 527 nm is not possible due to the excessive scatter from the heating pulse fundamental and the second harmonic generated during the interaction. This scattered light is rejected with an interference filter centered at the wavelength of the Raman shifted light. The back-lit target is imaged onto a charge coupled device camera. The estimated spatial resolution is 3 μm, and the time resolution is approximately 2 ps. The region that has undergone ionization to the critical density of 620 nm light ($n_e \sim 3 \times 10^{21}$ cm^{-3}) within the transparent glass slide becomes opaque to the probe.

The measured profile of the plasma at the target-vacuum interface at three different times is shown in Fig. 2. The peak laser intensity of the heating pulse was 0.8×10^{17} W/cm^2. The first image shows the plasma at a time roughly 3 ps before the peak of the pulse. ($t = 0$ is defined when we first observe the ionization wave propagate into the solid.) The second image shows the plasma at 6 ps after the heating pulse. An ionization front is clearly visible below the target surface. The plasma profile 14 ps after the heating pulse is shown in the final image. The ionization wave has expanded to an extent that is larger than the initially heated region of the focused spot. At this point the ionization expansion transforms from a one dimensional to a three dimensional expansion. Consequently, the rate of expansion slows dramatically.

We can determine the ionization wave velocity if we examine the maximum extent of the ionization wave in a direction normal to the target surface. This ionization front is plotted as a function of time in Fig. 3 for a peak intensity of 0.8×10^{17} W/cm^2. The ionization front propagates in with a supersonic velocity of approximately 6×10^8 cm/s. It then slows and saturates with a maximum penetration into the target after 15 ps of 90 μm. We can infer the average expansion velocity by fitting a line to the ionization front over the first $\sim$10 ps. This inferred velocity is plotted as a function of laser intensity in Fig. 4(a). The penetration depth after the expansion stops is plotted as a function of intensity in Fig. 4(b). We have defined this point at 25 ps after the heating pulse when the expansion has nearly stopped. The intensity was varied by changing the focused energy on the target. We have made previous measurements with a 1 ps pulse which suggest that the energy absorption is 40% for the pulses used in our experiments and is constant over the range of intensities used. The data in Fig. 4, therefore, essentially represent the velocity and penetration as a function of energy input into the plasma if we assume a constant absorption as a function of intensity.

Our measured expansion velocity of 8×10^8 cm/s at the highest intensity is nearly 2 orders of magnitude greater than the plasma sound velocity, $\sim 10^7$ cm/s (the velocity of an ionizing shock wave), and approximately 40 times greater than the supersonic ionization wave velocity reported at lower intensity in Ref. [5]. We can simply calculate the early ($<$30 ps) time history of the ionization front by finding the solution of the nonlinear heat diffusion equation. We assume the expansion is in one dimension at early times, and that the specific heat of the plasma is given by the ideal gas law. This will

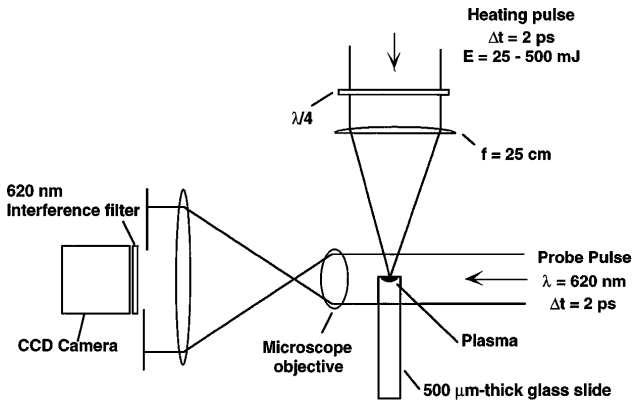

FIG. 1. Experimental setup to measure the dynamics of the ionization wave inside a solid target.

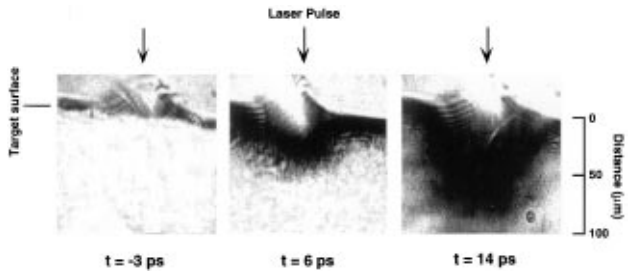

FIG. 2. Measured profile of the plasma at the target-vacuum interface at three times, (left) 3 ps before the heating pulse, (middle) 6 ps, and (right) 14 ps after the heating pulse.

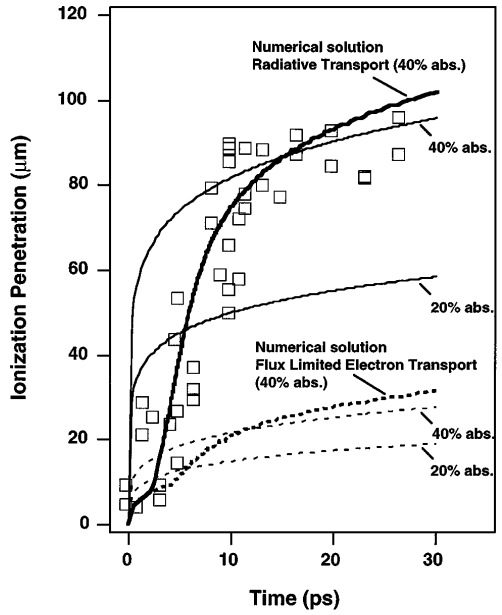

FIG. 3. Measured ionization front plotted as a function of time for a peak intensity of 0.8×10^{17} W/cm^2 (squares). The thin solid lines are the predictions of one dimensional radiative energy transport for 20% and 40% laser energy absorbed, and the dashed lines are for electron thermal transport. The thick solid line is the numerical calculation of the radiative energy transport in one dimension which includes the effects of flux-limited radiative heat flow. The thick dashed line is the numerical calculation for flux-limited electron transport (flux limiter = 0.5).

somewhat underestimate the actual specific heat since it ignores the energy required to ionize the target material. We seek the solution for the equation

$$\tfrac{3}{2}\, n_e k_B \frac{\partial T_e}{\partial t} = \frac{\partial}{\partial x}\left[\kappa(T_e)\frac{\partial T_e}{\partial x}\right], \qquad (2)$$

where $\kappa(T_e)$ is given by either the electron or radiative conductivity given above. The use of the diffusion equation to model the ionization front is appropriate because of the nature of the observed data. If the energy transport were dominated by nonlocal effects (such as hot electrons or hard x rays), we would expect to see prompt ionization within the solid target. Instead we observe the ionization front propagate with a speed significantly less than the speed of light, indicative of diffusive heat flow.

When a fast heat input is launched into a cold medium with a nonlinear heat conductivity, as is the case when a short-laser pulse heats the surface of a medium subject to either electron thermal or radiative heat conduction, Eq. (2) predicts the formation of a steep heat front propagating into the medium [12]. This heat front is characterized by a sharp rise in temperature whose leading edge is propelled into the cold material by the energy transport of the hot material from behind. Our experiment measures the maximum extent of ionization to the probe beam critical density ($\sim 3 \times 10^{21}$ cm^{-3}). This electron density will be achieved in fused silica when the plasma temperature has risen to $\sim$1 eV. Thus, the propagation distance of the observed ionization wave will correspond closely to the leading edge of this heat front and is a direct indicator of the extent of heat conduction by the hot material behind the heat front. An analytic solution of Eq. (2) exists for the extent of this temperature front for a delta function heat input [12]. This is closely approximated by our 2 ps heating pulse. For electron thermal conduction, the solution is [12]

$$x_{\text{front}}^{\text{SH}} = \xi_0 \left(\frac{8}{3m_e^{1/2}(Z+1)e^4 n_e^{7/2}\ln\Lambda}\right)^{2/9} F_{\text{abs}}^{5/9} t^{2/9}. \qquad (3)$$

F_{abs} is the absorbed laser energy fluence on the surface of the target. For radiative energy conduction the solution for the temperature front is [12]

$$x_{\text{front}}^{\text{rad}} = \xi_0 \left(\frac{32\sigma}{9 n_e^7 k_B^6 Z}\, 9 \times 10^6\right)^{1/7} F_{\text{abs}}^{5/7} t^{1/7}. \qquad (4)$$

To derive this we have used the simple formula for the Rossland mean free path quoted above. [ξ_0 is equal to 1.0 in Eq. (3) and is equal to 0.76 in Eq. (4).]

The estimates of the thermal ionization front for both electron thermal conduction and radiative conduction calculated from Eqs. (3) and (4) are compared in Fig. 3

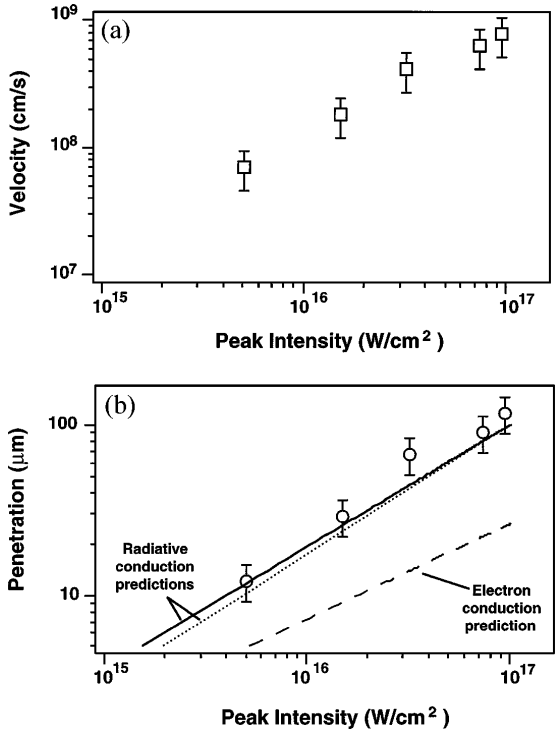

FIG. 4. (a) Inferred ionization front velocity plotted as a function of laser intensity. (b) Penetration depth after 25 ps plotted versus laser intensity. The solid line is the prediction of radiative energy transport, Eq. (4) with constant 40% laser energy absorption and the dashed line is the prediction of electron thermal conduction, Eq. (3). The dotted line is the prediction of the radiation transport numerical model.

with the measured ionization front for two values of the absorbed energy fraction 20% and 40%. We have assumed that the laser energy is deposited uniformly in a 20 μm Gaussian spot, and we have simply assumed $n_e \approx 10^{23}$ cm^{-3} (roughly solid density within the heated fused silica) to make quantitative estimates. (We have also assumed that $\ln\Lambda \approx 5$, appropriate for this plasma density and a plasma temperature of $\sim$500 eV.) Note that the one dimensional solutions of Eqs. (3) and (4) will generally overestimate the thermal front propagation distance since the experimental heat flow transforms from a one to three dimensional heat flow, slowing down the thermal wave due to volume increase. Even with these simplifying assumptions it is clear from the comparison in Fig. 3 that electron thermal conduction alone is inadequate in explaining the rapid expansion of the ionization front. The radiative heat flow model, however, does accurately predict the rapid expansion of the ionization front to $\sim$100 μm on a time scale of $\sim$20 ps.

The calculated extent of the ionization wave propagation after 25 ps assuming a fixed absorption fraction of 40% for both electron and radiative thermal conduction using Eqs. (3) and (4) is compared to the measured ionization wave penetration in Fig. 4(b). This comparison reinforces the importance of radiative heat conduction in the 10^{16} to 10^{17} W/cm^2 intensity range. Electron thermal conduction is inadequate in describing the deep penetration of the ionization wave on the fast time scale we have observed. Equation (4) accurately predicts the intensity scaling of the penetration depth, while the slope predicted by electron thermal conduction [Eq. (3)] is too shallow to explain the observed scaling.

From Fig. 3 we see that Eq. (4) clearly overestimates the propagation velocity at early time. This rapid propagation is due to the unphysical nature of the solution of Eq. (2) in which we have assumed a delta function heat input. This results in an infinite heat flux at $t = 0$ and an infinite velocity of the thermal wave at $t = 0$. In fact, the heat flux in an opaque plasma is clamped at its maximum possible value of $q_{\mathrm{rad}}^{\mathrm{max}} = \sigma T_e^4$ (in a manner analogous to the free streaming limit on the electron thermal heat flux of $q_{\mathrm{elec}}^{\mathrm{max}} = 3n_e v_{kT} k_B T_e/2$). For a sharp temperature gradient, this maximum heat flux implies a maximum thermal wave velocity of $v_{\mathrm{max}} \approx 2\sigma T_e^3/3k_B n_e$.

To explore this effect we have numerically solved Eq. (2) using radiative heat flow, accounting for the radiative heat flux limitation of σT_e^4. We have also used an estimate for Z as a function of temperature to more accurately estimate the electron density. To do this we have used the analysis of Ref. [6] which is based on a solution of the Saha equations. We have assumed that the energy input into the plasma occurs over a 2 ps pulse into a 2 μm deep region at the target surface. We have found, however, that the calculated time history is quite insensitive to the details of the energy deposition at the target surface, confirming the predictions of Eq. (4) which indicate that the important parameter is the absorbed energy fluence and not the specifics of the initial plasma temperature. The results of this calculation for an absorbed energy fraction of 40% are plotted in Fig. 3. This calculation accurately predicts the observed thermal wave velocity over the first 10 ps of the expansion as well as the rollover in the thermal wave penetration at $\sim$100 μm. The ionization front penetration after 25 ps calculated using this model is also shown in Fig. 4(b) as a dotted line. The numerical result is very close to the analytical result of Eq. (4).

For the sake of comparison we have also included the results of numerical calculations using standard flux-limited electron thermal transport in Fig. 3. For this we used a flux limiter of 0.5 (the maximum heat flux is clamped at $0.5 \times 3n_e v_{kT} k_B T_e/2$). We have found that the calculated curve changes very little when we vary the flux limiter between 0.1 and 1.0. The calculated ionization front velocity using electron thermal transport is over an order of magnitude lower than that of the data and is clearly inadequate in explaining the observed rapid penetration of the ionization front.

In conclusion, we have presented the first direct measurement of radiation driven ionization waves in short-pulse produced plasmas. We find that at an intensity of 10^{17} W/cm^2 the ionization wave exhibits a supersonic velocity of expansion into fused silica of nearly 10^9 cm/s. The ionization wave penetrates to a depth of $\sim$100 μm into the cold substrate on a time scale of $<$20 ps. This measurement suggests that there is a transition from an electron to radiation transport mechanism as the intensity of short-pulse irradiation increases from 10^{14} to 10^{17} W/cm^2.

We would like to acknowledge useful conversations with O. Willi, and we appreciate the technical assistance of S. Haniff. R. A. Smith is supported by an EPSRC Advanced Fellowship.

[1] M. D. Perry and G. Mourou, Science **264**, 917 (1994).
[2] C. Y. Chien *et al.*, Opt. Lett. **18**, 1535 (1993).
[3] H. M. Milchberg *et al.*, Phys. Rev. Lett. **67**, 2654 (1991).
[4] M. M. Murnane *et al.*, Phys. Rev. Lett. **62**, 155 (1989).
[5] B. T. Vu *et al.*, Phys. Rev. Lett. **72**, 3823 (1994).
[6] B. T. Vu *et al.*, Phys. Plasmas **2**, 476 (1995).
[7] P. D. Gupta *et al.*, Phys. Rev. A **34**, 4103 (1986).
[8] R. Sigel *et al.*, Phys. Rev. A **45**, 3987 (1992).
[9] V. J. L. White *et al.*, Phys. Rev. E **49**, R4803 (1994).
[10] T. Afshar-rad *et al.*, Phys. Rev. Lett. **73**, 74 (1994).
[11] L. Spitzer and R. Härm, Phys. Rev. **89**, 977 (1953).
[12] Y. B. Zel'dovich and Y. P. Raizer, Physics of Shock Waves and High-Temperature Hydrodynamic Phenomena, edited by W. D. Hayes and R. F. Probstein (Academic Press, New York, 1966).